

1
2
3
4
5
6
7
8
9
10
11
12
13
14
15
16
17
18
19
20
21
22
23
24
25

***Tyr* is Responsible for the *Cctq1a* QTL and Links Developmental Environment to Central Corneal Thickness Determination**

Kacie J. Meyer^{1§}, Demelza R. Larson^{1§}, S. Scott Whitmore², Carly J. van der Heide^{1,2}, Adam Hedberg-Buenz^{1,3}, Laura M. Dutca³, Swanand Koli⁴, Nicholas Pomernackas¹, Hannah E. Mercer¹, Maurisa N. Mansaray¹, William J. Paradee⁵, Kai Wang⁶, K. Saldas Nair^{4,7}, Todd E. Scheetz², and Michael G. Anderson^{1,2,3*}

¹Department of Molecular Physiology and Biophysics, University of Iowa, Iowa City, Iowa;

²Department of Ophthalmology and Visual Sciences, University of Iowa, Iowa City, Iowa;

³Center for the Prevention and Treatment of Visual Loss, Iowa City VA Health Care System,

Iowa City, Iowa; ⁴Department of Ophthalmology, University of California, San Francisco,

California; ⁵Genome Editing Core Facility, University of Iowa, Iowa City, Iowa; ⁶Department of

Biostatistics, University of Iowa, Iowa City, Iowa; ⁷Department of Anatomy, University of

California, San Francisco, California

[§]Equal contribution

*Corresponding author: Dr. Michael G. Anderson, Department of Molecular Physiology and Biophysics, 3123 Medical Education and Research Facility, 375 Newton Road, Iowa City, IA 52242, (319) 355-7839 (telephone), (319) 335-7330 (FAX), michael-g-anderson@uiowa.edu

26 **Abstract**

27

28 Central corneal thickness is a quantitative trait with important associations to human health. In a
29 phenotype-driven approach studying corneal thickness of congenic derivatives of C57BLKS/J
30 and SJL/J mice, the critical region for a quantitative trait locus influencing corneal thickness,
31 *Cctq1a*, was delimited to a 10-gene interval. Exome sequencing, RNAseq, and studying
32 independent mutations eliminated multiple candidate genes and confirmed one. Though the
33 causative gene, *Tyr*, has no obvious direct function in the transparent cornea, studies with
34 multiple alleles on matched genetic backgrounds, both in isolation and genetic complementation
35 crosses, confirmed allelism of *Tyr-Cctq1a*; albino mice lacking *Tyr* function had thin corneas.
36 Albino mice also had increased axial length. Because albinism exposes eyes to increased light,
37 the effect of dark-rearing was tested and found to rescue central corneal thickness. In sum, the
38 results point to an epiphenomenon; developmental light exposure interacts with genotype as an
39 important determinate of adult corneal thickness.

40 **Introduction**

41

42 Central corneal thickness has important associations with ocular disease, but its natural
43 determining factors remain predominately elusive. The cornea consists of three cellular layers
44 (an outermost epithelium, middle stroma, and innermost endothelium) separated by two thinner
45 basement membranes. The combined central thickness of these layers (central corneal
46 thickness, CCT) increases rapidly through infancy and early childhood, reaches adult values in
47 pre-teen ages, and remains relatively stable thereafter, with eventual modest age-related
48 thinning^{1, 2, 3, 4}. For largely unknown reasons, average CCT can vary by dozens of microns
49 between ethnicities^{4, 5}. Thin CCT is associated with several corneal diseases, such as corneal
50 dystrophy, brittle cornea syndrome, keratoconus, and cornea plana; diseases of connective
51 tissue, such as Marfan syndrome, Ehlers-Danlos syndrome, Loeys-Dietz syndrome, and
52 osteogenesis imperfecta; and at least two diseases in which the nature of, and/or reason for, the
53 association is unclear, including myopia and primary open angle glaucoma⁶.

54

55 CCT is a highly heritable trait^{7, 8}, leading to many genetic studies. Variants influencing CCT have
56 been identified from familial studies of Mendelian syndromes and GWAS of various large
57 populations^{9, 10, 11, 12}. From these studies, some themes have begun to emerge. For example,
58 some of the same CCT loci are identified in both multigenic and Mendelian disease studies^{10, 13,}
59 ¹⁴. It has also been common to identify variants related to collagen matrix integrity^{10, 12, 14, 15}.

60 However, it is also clear that much remains unknown. Among the known associations, most
61 known SNPs occur in non-coding regions, and the nearest genes typically have no obvious link
62 to known structural components of the cornea¹⁵. It is also clear that many important genes
63 remain to be discovered. Known SNPs give rise to a SNP-based heritability estimate of 42.5%
64 and account for only 14.2% of the CCT variance⁹.

65
66 Here, an unique approach complementary to others is undertaken using inbred mouse strains to
67 identify quantitative trait loci (QTL) that influence CCT¹⁶. Similar to humans, there is natural
68 variation of CCT among inbred mouse strains¹⁷. Previous work using a quantitative approach
69 with intercrosses between two such strains (C57BLKS/J [KS] mice with thin corneas and SJL/J
70 [SJL] mice with thick corneas) identified the first CCT QTL, *Central corneal thickness QTL 1*
71 (*Cctq1*) on mouse chromosome 7¹⁶. Here, *Cctq1* was resolved into two closely linked regions,
72 *Cctq1a* and *Cctq1b*, which each influence CCT. Through multiple genetic approaches, a
73 mutation in the tyrosinase gene (*Tyr*) is identified as causative of the *Cctq1a* phenotype, which
74 appears to influence CCT via an epiphenomenon dependent on developmental light exposure.

75

76 **Results**

77

78 ***Cctq1* contains two adjacent interacting QTL**

79 The original 95% Bayesian credible interval of *Cctq1* spanned a 38.3 cM region on chromosome
80 7 (34.1 cM – 72.4 cM)¹⁶. To reduce this interval, recombination mapping was used with 92
81 recombinant N4 intercross mice. However, the interval was originally recalcitrant to division—
82 more than one interval conferred the increased CCT phenotype. This suggested that there was
83 too much genetic heterogeneity for this trait at the N4 generation, potentially including the
84 presence of more than one CCT-regulating gene within or near *Cctq1*. To address these
85 possibilities, the original F2 dataset was subjected to additional evaluations while backcrossing
86 of the congenic mice to the N10 generation was continued.

87

88 The original analysis of (KS X SJL) F2 mice was based upon a significance threshold
89 determined empirically by stratified permutation testing with 1000 permutations^{16, 18}, and did not
90 identify any loci that significantly interacted with *Cctq1*. Prompted by the recombination

91 mapping, the dataset was re-examined by performing a pairwise scan of the markers on
92 chromosome 7 using scantwo analysis with R/qtl^{18, 19}. Of the possible interactions, the markers
93 that produced the highest LOD scores were *D7Mit31* and *rs13479535* (Figure 1A; full LOD
94 score = 10.33, interactive LOD score = 5.05). *D7Mit31* lies within the 95% Bayes credible
95 interval of *Cctq1*; *rs13479535* is 2 cM distal to the end of the interval at 74.3 cM. The putative
96 linked loci were subsequently subjected to multiple regression analysis in which each locus and
97 the interaction component were sequentially dropped from the 2-QTL model. This analysis
98 indicated that both loci and their interaction had significant contributions to the model
99 (Supplementary Data 1). The QTL at *D7Mit31* was responsible for 31% of the phenotypic
100 variability while the QTL at *rs13479535* accounted for another 24% of the variability. These data
101 indicate that both loci are true QTL. *Cctq1* was thus resolved into two QTL, *Cctq1a* (95% Bayes
102 credible interval: *D7Mit318–D7Mit220*, spanning 49.0 cM, peak at *D7Mit31*), and *Cctq1b* (95%
103 Bayes credible interval: *D7Mit105–rs13479545*, spanning 74.3 cM, peak at *rs13479535*; Figure
104 1B).

105
106 To reduce genetic heterogeneity, N4 mice were further backcrossed onto the KS background to
107 the N10 generation. Because the congenic interval was relatively large, a panel of six markers
108 was used at each generation of backcrossing to keep the interval intact. At generation N10,
109 congenic mice were intercrossed, recombination within the interval was allowed, and mice with
110 all nine genetic combinations of *Cctq1a* and *Cctq1b* were phenotyped for CCT (Table 1).
111 Congenic control mice (KS.SJL-*Cctq1a*^{KS}, *Cctq1b*^{KS}) had a CCT indistinguishable from inbred
112 KS mice (94.8 ± 2.4 μm vs. 94.5 ± 3.2 μm, respectively; one-way ANOVA with Tukey post-test;
113 Table 1). Congenic mice with SJL genotypes at *Cctq1a* (i.e., KS.SJL-*Cctq1a*^{SJL}) had significantly
114 thinner corneas than inbred KS mice (87.9 ± 3.8 μm; *n* = 39; *p* < 0.001; Student's two-tailed *t*-
115 test) independent of the genotype at *Cctq1b* (*n* = 13 and *p* < 0.05 for each of three genotypes at
116 *Cctq1b*; one-way ANOVA with Tukey post-test; Table 1; Supplementary Data 2). The difference

117 in thickness mediated by *Cctq1a* is predominantly due to the thickness of the stroma (Δ 9.6 μm ,
118 $p < 0.001$; Student's two-tailed *t*-test), though there is a small (Δ 1.2 μm) and marginally
119 significant ($p = 0.022$ Student's two-tailed *t*-test) decrease in thickness of the epithelium as well.
120 Congenic mice with KS genotypes at *Cctq1a* and SJL genotypes at *Cctq1b* (i.e., KS.SJL-
121 *Cctq1a*^{KS}, *Cctq1b*^{SJL}) also had significantly thinner corneas ($90.8 \pm 2.6 \mu\text{m}$; $n = 13$ mice; $p < 0.05$;
122 one way ANOVA with Tukey post-test) than inbred KS mice (Table 1, Supplementary Data 2).
123 No other genetic combinations caused significant changes in CCT compared to inbred KS
124 controls. As predicted from the analysis of the original F2 Dataset with R/qtl, these data with
125 congenic mice independently support that both *Cctq1a* and *Cctq1b* are true QTL capable of
126 altering the phenotypic variability of CCT on a uniform genetic background.

127

128 **Mapping of *Cctq1a* using recombination mapping and sub-congenics**

129 Because of its larger effect, initial efforts were focused on fine-scale mapping for *Cctq1a*. To
130 identify the gene underlying *Cctq1a*, *Cctq1a*-recombinant N10F2 mice, with KS genotypes at
131 *Cctq1b*, were used to narrow the critical region. From this recombination analysis, the gene
132 underlying *Cctq1a* was deduced to be between SNP markers *rs108403472* at 48.51 cM and
133 *rs6247100* at 50.26 cM. Simultaneously, sub-congenic mice were created by continued
134 backcrossing of the KS.SJL-*Cctq1a*^{HET}; *Cctq1b*^{KS} N10 mice. Eyes of N10 congenic mice were
135 overtly healthy, differing only in pigmentation between genotypes (Supplementary Data 2). At
136 N12, *Cctq1a* was physically reduced to a 15.9 cM region (KS.SJL-*Cctq1a*(15.9cM)) flanked by
137 *D7mit347* and *D7mit321* and characterized by an association of SJL homozygosity with
138 decreased CCT ($87.6 \pm 2.3 \mu\text{m}$ vs. $76.8 \pm 2.4 \mu\text{m}$, $n = 15$ mice per genotype, $p < 0.001$,
139 Student's two-tailed *t*-test). At N15, *Cctq1a* was physically reduced to a 9.9 cM region (KS.SJL-
140 *Cctq1a*(9.9cM)) flanked by *rs3672782* and *D7mit321*; again characterized by an association of
141 SJL homozygosity with decreased CCT ($91.6 \pm 2.2 \mu\text{m}$ vs. $80.7 \pm 2.9 \mu\text{m}$, $n = 7$ mice per
142 genotype, $p < 0.001$, Student's two-tailed *t*-test). One N15F2 mouse harbored a recombination

143 event within the minimal sub-congenic interval. The phenotype of this mouse indicated the gene
144 underlying *Cctq1a* lies proximal to marker *rs13479393* (Figure 2). Using this recombinant
145 mouse in a progeny test, additional intercrossing to generation N15F7 confirmed the distal
146 breakpoint proximal to marker *rs13479393* at 49.65 cM, again characterized by an association
147 of SJL homozygosity with decreased CCT ($85.7 \pm 1.6 \mu\text{m}$ vs. $94.4 \pm 3.3 \mu\text{m}$, $n = 8\text{--}10$ mice per
148 genotype; $p < 0.001$, Student's two-tailed *t*-test; Figure 3A; Supplementary Data 3–5).

149
150 In sum, physical recombination mapping utilizing multiple generations of congenic and sub-
151 congenic mice conclusively indicated that the gene underlying *Cctq1a* lies on chromosome 7
152 between markers *rs108403472* at 48.51 cM and *rs13479393* at 49.32 cM, a 0.81 cM region
153 containing the entirety of eight RefSeq genes (*Vmn2r78*, *Vmn2r79*, *Nox4*, *Tyr*, *Grm5*, *Ctsc*,
154 *Rab38*, and *Tmem135*), the 3' portion of one gene (*Vmn2r77*), and the 5' portion of one gene
155 (*Fzd4*) (Figure 2).

156

157 **Candidate identification and prioritization**

158 To identify all the possible exonic variants within the *Cctq1a* critical region, whole exome
159 sequencing was conducted on KS and SJL inbred mice. In the entire exome, 15,261 missense,
160 frameshift, and splice-site mutations were found between KS and SJL (Supplementary Data 6).

161 There were six amino acid altering variants within the *Cctq1a* critical region, located within
162 *Vmn2r79* (A223T, L243M, T257I, I265V), *Tyr* (C103S), and *Fzd4* (F27L). Vomeronasal receptor
163 genes, such as *Vmn2r79*, have an increased rate of coding sequence variants²⁰ and the four
164 altered residues between KS and SJL in *Vmn2r79* are poorly conserved. The amino acid
165 change in *Tyr* from cysteine to serine is the albinism-causing *Tyr^c* allele conferred by the albino
166 SJL strain. The *Fzd4* amino acid variant is within the signal sequence of the protein; KS mice
167 conferred the phenylalanine amino acid residue (the same residue as C57BL/6J mice) while
168 SJL mice conferred the mammalian-conserved leucine residue.

169

170 Transcriptional profiling was additionally used to prioritize candidates. Using previously
171 published microarray data comparing adult corneal RNA expression profiles in KS and SJL
172 mice¹⁷, *Nox4*, *Ctsc*, *Rab38*, *Tmem135*, and *Fzd4* were all present in the adult cornea; there was
173 no evidence for adult corneal expression of *Vmn2r77*, *Vmn2r78*, *Vmn2r79*, *Tyr*, or *Grm5*. Of
174 those expressed, *Nox4*, *Ctsc*, and *Fzd4* showed differential expression between the two strains.
175 *Nox4* and *Ctsc* were both down-regulated 2.5-fold in SJL, while *Fzd4* was up-regulated 1.6-fold
176 in SJL.

177

178 Additionally, RNAseq was performed on corneas of 3-week-old KS.SJL-*Cctq1a*(15.9cM)^{SJL}
179 N12F3 mice. Analysis was focused on three comparisons: 1) KS.SJL-*Cctq1a*(15.9cM)^{SJL} vs. KS
180 (experimental, identifying genes with altered corneal expression in the congenic interval), 2)
181 KS.SJL-*Cctq1a*(15.9cM)^{SJL} vs. KS.SJL-*Cctq1a*(15.9cM)^{KS} (experimental, also identifying genes
182 with altered corneal expression in the congenic interval), and 3) KS.SJL-*Cctq1a*(15.9cM)^{KS} vs.
183 KS (control, identifying genes in the background of the congenic strain with altered corneal
184 expression not associated with the congenic interval) (Supplementary Data 7). In each
185 comparison, genes were first filtered for those with a Q-value ≤ 0.001 and a FPKM ≥ 1 in at
186 least one of the strains. Gene lists were subsequently compared to one another, identifying 87
187 genes consistently altered in both experimental comparisons but not in the control comparison
188 (Supplementary Data 7). Among these 87, only one was localized to the *Cctq1a* critical region,
189 *Ctsc*, which was modestly ($-0.8 \log_2$ fold) but consistently and significantly ($p = 5 \times 10^{-5}$; $Q =$
190 0.0009) down regulated in comparing the SJL allele to the KS allele. Web Gestalt²¹ was used for
191 over-representation analysis comparing the list of 87 differentially expressed genes to a
192 background list of all genes expressed in the cornea with a FPKM ≥ 1 in any strain. Results of
193 the analysis indicate a strong signal for several collagen-related categories (fibrillar collagen
194 trimer, abnormal cutaneous collagen fibril morphology, collagen biosynthesis and modifying

195 enzymes, collagen degradation, etc.), extracellular-matrix-related categories (extracellular
196 matrix component, ECM proteoglycans, degradation of the extracellular matrix, etc.) and ocular-
197 related categories (decreased corneal stroma thickness, abnormal corneal epithelium
198 morphology, abnormal cornea morphology, and abnormal eye morphology) (Supplementary
199 Data 8).

200

201 **Functional tests of lead candidates**

202 Based on candidate prioritization criteria, *Fzd4* and *Ctsc* were initially considered the top
203 candidates. To test the influence of *Fzd4* on CCT, we tested a strain with a targeted mutation of
204 *Fzd4* (B6;129-*Fzd4*^{tm1Nat}/J) on a segregating B6 and 129 background²². *Fzd4*^{tm1Nat} homozygotes
205 had a chocolate coat color not expected from either background. This observation is meaningful
206 as the gene responsible for this phenotype, *Rab38*, is physically near *Fzd4* and within the *Cctq1*
207 critical region, i.e., the strain is likely a double mutant for *Fzd4* (genotype verified) and *Rab38*
208 (mutation unknown). However, there was no correlation between *Fzd4*^{tm1Nat} genotype and CCT
209 ($p = 0.819$; one-way ANOVA comparing all three genotypes among littermates; Figure 3B;
210 Supplementary Data 3–5). In genetic complementation crosses, *Fzd4*^{tm1Nat} mutation
211 complemented the congenic interval ([*Fzd4*^{WT}/*Cctq1a*^{SJL} F1] vs. [*Fzd4*^{HET}/*Cctq1a*^{SJL} F1]; $p =$
212 0.528 ; Student's two-tailed *t*-test; $n = 4-6$ per genotype; Figure 3C; Supplementary Data 3–5).
213 The complementation cross also highlighted the coat color phenotype associated with the
214 *Fzd4*^{tm1Nat} mutation, with *Fzd4*^{WT}/*Cctq1a*^{SJL} F1 mice (*Tyr*^{HET}) having a black coat color with
215 normally pigmented eyes and *Fzd4*^{HET}/*Cctq1a*^{SJL} F1 mice (*Tyr*^{HET}) having an unmistakable
216 lightened (“light chocolate”) coat color and light brown irides instead of brown (Supplementary
217 Data 9). Therefore, *Fzd4* was ruled out as causative of the *Cctq1a* phenotype, and *Rab38*
218 further deprioritized as a candidate.

219

220 To test the influence of *Ctsc* on CCT, we imported a strain with a targeted mutation of *Ctsc*
221 (B6.Cg-*Ctsc*^{tm1Ley}) on an N10 congenic B6 background²³. Because the targeted mutation was
222 generated on an albino 129 background, and *Ctsc* is physically linked to *Tyr*, *Ctsc*^{tm1Ley}
223 homozygotes are albino, i.e., the strain is a double mutant for *Ctsc* and *Tyr*. This is meaningful
224 because the SJL/J strain is albino and the *Tyr*^c mutation is within the KS.SJL-*Cctq1a* congenic
225 interval. Homozygotes had a statistically significant decrease in CCT compared to littermate
226 controls ($p < 0.002$ for albino *Ctsc*^{tm1Ley} vs. pigmented *Ctsc*^{HET}; $p < 0.002$ for albino *Ctsc*^{tm1Ley} vs.
227 pigmented *Ctsc*^{WT}; one-way ANOVA with Tukey post-test comparing all three genotypes among
228 littermates; $n=10-12$ mice per genotype; Figure 3D; Supplementary Data 3-5). In genetic
229 complementation crosses, *Ctsc*^{tm1Ley} failed to complement *Cctq1a*^{SJL} ($p < 0.001$ for pigmented
230 [*Ctsc*^{tm1Ley}/*Cctq1a*^{KS} F1] vs. albino [*Ctsc*^{tm1Ley}/*Cctq1a*^{SJL} F1]; Student's two-tailed *t*-test; $n = 10-$
231 11 mice per genotype; Figure 3E; Supplementary Data 3-5). Therefore, *Ctsc* or *Tyr* were
232 determined to be causative of the *Cctq1a* phenotype.

233
234 To differentiate *Ctsc* and *Tyr* as the causative mutation, independent alleles on a pure B6
235 background were assessed. To test *Ctsc*, four new mutations predicted to result in null protein
236 were generated in B6 mice with CRISPR-Cas9 technology (Supplementary Data 10). To test
237 *Tyr*, a well-known spontaneous mutation that was commercially available, *Tyr*^{c-2J}, was
238 analyzed^{24, 25}. There was no association between *Ctsc*^{KO} genotype and CCT ($p = 0.237$; one-
239 way ANOVA comparing all three genotypes among littermates; $n = 9-17$ mice per group; Figure
240 3F; Supplementary Data 3-5). In genetic complementation crosses with the congenic strain, the
241 *Ctsc*^{tm1Mga} mutation (46bp-deletion in the coding sequence of exon 1 leading to no detectable
242 CTSC protein; Supplementary Data 10) complemented the congenic phenotype ($p = 0.696$;
243 Student's two-tailed *t*-test; $n = 8-12$ mice per group; Figure 3G; Supplementary Data 3-5). In
244 contrast, albino *Tyr*^{c-2J} mice had decreased CCT relative to pigmented B6 ($p < 0.001$; Student's
245 two-tailed *t*-test; $n = 9-10$ mice per group; Figure 3H; Supplementary Data 3-5). In genetic

246 complementation crosses with the congenic strain, the Tyr^{c-2J} mutation failed to complement the
247 congenic phenotype ($p < 0.001$ for pigmented [$Cctq1a^{KS}/Tyr^{c-2J}$ F1] vs. albino [$Cctq1a^{SJL}/Tyr^{c-2J}$
248 F1]; Student's two-tailed t -test; $n = 8$ mice per genotype; Figure 3I; Supplementary Data 3–5).
249 Thus, only Tyr mutation was left as a feasible candidate for $Cctq1a$.

250
251 CRISPR-Cas9 technology was also used to generate new Tyr mutations on a C57BL/6J
252 background (Supplementary Data 11). One allele was selected for propagation, Tyr^{tm4Mga} , an
253 albinism-causing 4bp-deletion in the coding sequence of exon 1 that is predicted to cause a
254 frameshift leading to a premature stop codon and RNA-mediated decay; i.e., a presumed null
255 mutation. Tyr^{tm4Mga} mice had a significantly thinner cornea than littermate controls ($p < 0.002$ for
256 Tyr^{WT} vs. Tyr^{tm4Mga} ; $p < 0.002$ for Tyr^{HET} vs. Tyr^{tm4Mga} ; one-way ANOVA with Tukey post-test
257 comparing all three genotypes among littermates; $n = 6$ –10 mice per genotype; Figure 4;
258 Supplementary Data 5 and 12). Thus, a presumed null allele of Tyr caused the same albinism
259 and thinning of CCT as found for the c and $c-2J$ alleles.

260

261 **Mechanism of Tyr function on CCT**

262 In considering the possible mechanism through which Tyr might influence CCT, three
263 hypotheses were tested:

264

265 The first candidate mechanism centered on the role of DOPA, which is a cofactor in the
266 oxidation of tyrosine by TYR, leading to melanin production²⁶, and a substrate for tyrosine
267 hydroxylase (TH), leading to dopamine synthesis. Dopamine is considered a key molecule in
268 ocular growth^{27, 28}, and mice with a conditional knock-out of Th in the retina have previously
269 been shown to have decreased CCT²⁹. Rationalizing that some DOPA may normally escape
270 from pigment producing cells to influence CCT via a TH-dependent mechanism, we tested
271 whether providing supplemental DOPA in the drinking water of albino mice would rescue the

272 decreased CCT associated with albinism. No statistically significant effect was observed (Figure
273 5; Supplementary Data 5), discounting the hypothesis that a DOPA deficit was rate-limiting for
274 CCT determination in *Tyr* mutant mice.

275
276 The second candidate mechanism revolves around the possibility of a gene-environment
277 interaction involving temperature and light. In this series of experiments, mice were reared in
278 environmental control chambers in combinations of different temperatures and light cycles.
279 Cohorts included pigmented B6, albino *Tyr^{c-2J}*, and the temperature sensitive himalayan
280 mutation (B6.Cg-*Tyr^{c-h}/J*)^{30,31}. At ambient temperatures, *Tyr^{c-h}* homozygotes are only partially
281 pigmented on the coolest parts of the body (such as the ears, nose, tail, and eyes) and CCT is
282 intermediate between B6 and *Tyr^{c-2J}* mice (Supplementary Data 5, 13, and 14). For CCT of mice
283 raised at ambient temperature, genetic complementation tests again confirmed the influence of
284 *Tyr*-mediated albinism on CCT ($p = 0.337$ for [pigmented B6 x *Tyr^{c-h}* F1] vs. [pigmented B6 x
285 *Tyr^{c-2J}* F1]; $p < 0.002$ for [pigmented B6 x *Tyr^{c-h}* F1] vs. [albino *Tyr^{c-h}* x *Tyr^{c-2J}* F1]; and $p < 0.002$
286 for [pigmented B6 x *Tyr^{c-2J}* F1] vs. [albino *Tyr^{c-h}* x *Tyr^{c-2J}* F1]; one-way ANOVA with Tukey post-
287 test; $n = 4-14$ mice per group, Supplementary Data 5). At decreased temperatures *Tyr^{c-h}*
288 homozygotes can generate pigment more broadly, and at increased temperatures the albinism
289 is accentuated (Supplementary Data 13 and 14).

290
291 Regarding temperature, comparison of B6. *Tyr^{c-h}* mice, as well as B6 and B6. *Tyr^{c-2J}* controls,
292 raised at 10°C vs. 32°C in environmental control chambers with a standard light cycle, showed
293 that CCT followed pigment status; the thin CCT of hypopigmented *Tyr^{c-h}* mice reared at
294 increased temperature (i.e., lower TYR activity) was rescued by rearing the *Tyr^{c-h}* mice at
295 decreased temperature (i.e., higher TYR activity; *Tyr^{c-h}* at 32°C vs. *Tyr^{c-h}* at 10°C; $\Delta 10.9 \mu\text{m}$; p
296 < 0.001 ; $n = 13-15$ mice per condition; one-way ANOVA with Sidak test; Figure 6;
297 Supplementary Data 5). In testing the effect of temperature on corneal thickness in controls,

298 there was a small (Δ 2.8 μm) and nominally significant ($p = 0.03$) decreased CCT in mice raised
299 at 10°C compared to mice raised at 32°C when considering all C57BL/6J and *Tyr^{c-2J}* mice
300 across the experiment ($n = 16$ mice vs. $n = 19$ mice, Type II ANOVA) and there was no
301 interaction between genotype and temperature. In sum, changing environmental temperature
302 changed CCT of the *Tyr^{c-h}* mice as predicted.

303

304 Regarding light, comparison of B6.*Tyr^{c-h}* mice, as well as B6 and B6.*Tyr^{c-2J}* controls, raised at
305 10°C vs. 32°C in environmental control chambers with dark-rearing of mice from conception to
306 10–15 weeks of age rescued the thin CCT phenotype associated with albinism ($p < 0.001$ for
307 [*Tyr^{c-h}* at 32°C standard light] vs. [*Tyr^{c-h}* at 32°C dark rear]; $p < 0.03$ for [*Tyr^{c-2J}* at 10°C standard
308 light vs. *Tyr^{c-2J}* at 10°C dark rear]; $p < 0.001$ for [*Tyr^{c-2J}* at 32°C standard light vs. *Tyr^{c-2J}* at 32°C
309 dark rear]; $n = 5$ –16 per condition; one-way ANOVA with Sidak test; Figure 6; Supplementary
310 Data 5). Rearing pigmented B6 mice in constant light is known to lead to an increase in axial
311 length³². OCT examinations of independent cohorts of C57BL/6J and *Tyr^{c-2J}* mice for the
312 purpose of measuring axial length show that *Tyr^{c-2J}* mice have a 65.6 μm greater axial length on
313 average compared to C57BL/6J mice (3.453 mm vs. 3.388 mm, respectively; $p < 0.001$,
314 Student's two-tailed *t*-test; $n = 10$ male and 10 female mice per strain; Figure 7).

315

316 Discussion

317 Using a phenotype-driven quantitative genetic analysis of CCT, physical mapping led to
318 identification of a small critical region containing 10 genes, of which we ruled out three (*Fzd4*,
319 *Rab38*, *Ctsc*) and found via an analysis of a *Tyr* allelic series (*c*, *c-2J*, *c-h*) that *Tyr* is the
320 causative gene underlying the *Cctq1a* QTL. *Tyr* is by no means an unknown gene—it was in
321 fact one of the first known mammalian genes whose initial discovery predates the word “gene”²⁶,
322 ^{33, 34}. However, *Tyr* was a surprising gene to find linked to CCT. TYR is an oxidase whose only
323 known biological role relates to melanin synthesis^{26, 35}. Although there are small numbers of

324 pigmented cells in the corneal limbus, the cornea is by and large not only non-pigmented, but
325 transparent. Furthermore, previously published data indicate that *Tyr* is not even expressed in
326 the adult cornea¹⁷, which is consistent with the current study which also found near-zero
327 expression in the cornea at 3 weeks of age (RNA-Seq max expression ~1.3 FPKM;
328 Supplementary Data 7). Thus, there is no molecular rationale for proposing that TYR has a
329 direct function in corneal cells. If not for the current experiments, there would also be sparse
330 biological rationales for proposing that TYR might influence corneal anatomy through any
331 mechanism. Regardless, the current agnostic QTL study led to the conclusion that *Tyr*
332 contributes to the primary genetic influence on CCT, at least in the context of KS x SJL hybrids.
333 Experiments using multiple alleles on matched genetic backgrounds, in isolation and genetic
334 complementation crosses, conclusively confirmed allelism of *Tyr-Cctq1a*; albino mice lacking
335 TYR function have thin corneas. Rationalizing that albinism would expose the developing eye to
336 increased light, one of the mechanistic experiments performed here compared the effect of
337 dark-rearing on the CCT of albino vs. pigmented C57BL/6J mice. The results showed that the
338 thin CCT phenotype of albino B6. *Tyr^{c-h}* mice raised at 32°C and B6. *Tyr^{c-2J}* mice was rescued by
339 dark-rearing. Thus, we are led to propose an epiphenomenon, whereby developmental light
340 exposure interacts with genotype as an important determinate of corneal thickness.

341
342 All current CCT measurements were done with mice 10–15 weeks of age, which is slightly past
343 the age at which the cornea of B6 mice reaches its final adult thickness (~P55)³⁶. Transcriptomic
344 changes in the cornea related to *Tyr* genotype were detectable at 3 weeks of age. Thus, the
345 timeframe for when *Tyr* can impact the cornea is presumably during anterior chamber
346 development at some point preceding 3 weeks of age. Two mechanisms, which are both
347 conjectural, might feasibly contribute to this early acting phenomenon. 1) Corneal development
348 might be a component of refractive development. Emmetropization typically occurs in the first
349 months following eyelid opening, with impacts from both the amount of light and its focus on the

350 retina^{32,37}. Thus, it is feasible that albinism could in effect cause blur (from light not being
351 absorbed by melanin and reflecting within the eye), which induces relative myopia and CCT
352 thinning with rearing in normal lights, but not in dark-rearing. 2) Corneal development might be
353 influenced by central or corneal circadian outputs. Circadian outputs arise from both central and
354 peripheral clocks, with the suprachiasmatic nucleus (SCN) being a central master pacemaker
355 that receives light signals from retinal ganglion cells and subsequently coordinates phasing to
356 peripheral tissues^{38,39}. Notably, the SCN receives retinal input from the retinohypothalamic tract,
357 which is known to be expanded in albinos^{40,41,42}. Thus, one possibility is that factors increasing
358 SCN output (such as albinism or cycling light conditions) might lead to decreased CCT and
359 those decreasing the signaling (such as dark rearing) might lead to increased CCT. Refractive
360 and circadian mechanisms could also be acting in an intertwined way⁴³. Additional experiments
361 are needed to distinguish these, and possibly other, mechanisms relevant to our current
362 findings.

363
364 A leading candidate for contributing to the molecular mechanism causing thin CCT in albino
365 mice was DOPA, which is a cofactor for TYR^{26,35}, a substrate for TH leading to dopamine
366 (reviewed in²⁷), and an endogenous ligand for the G-protein-coupled receptor GPR143⁴⁴.
367 DOPA can modulate refractive development^{27,29,40} and the circadian system⁴⁵, as well
368 development of multiple ocular tissues^{46,47}. Notably, mice with a conditional knock-out of *Th* in
369 the retina have decreased CCT²⁹. The current experiments with *Tyr* mutant mice were not able
370 to detect a role for DOPA in influencing CCT of these albino strains, though an important caveat
371 to point out is that only a single dosing schedule for DOPA supplementation was currently
372 tested.

373
374 It is unclear whether albinism or pigmentation influences CCT in humans, though our current
375 experiments suggest this is likely. In humans, loss of function mutations in *TYR* cause

376 oculocutaneous albinism type 1 (OCA 1)^{35, 48}. It's unclear from the literature if humans with OCA
377 1 have decreased CCT; it may be difficult to ascertain because of relatively small patient
378 populations and confounding variables such as eye rubbing⁴⁹.

379

380 The current study has several implications with respect to mouse genetics and mouse models of
381 disease: 1) The results highlight the potential for environmental influences on ocular
382 development, which have been quantitated here for CCT, but may extend to other tissues as
383 well. 2) The results indicate that albino mice should be tested for potentially being a naturally
384 occurring model of myopia. 3) Because CCT is a complex trait, there is little reason to suspect
385 that different inbred albino mouse strains would necessarily have the thinnest CCT in
386 comparison to other inbred strains that are pigmented⁵⁰, only that they would have thinner CCT
387 as albino mice compared to pigmented mice *within* an inbred strain. However, for any
388 experiment using such an albino strain, or cohorts in which an allele such as the common *Tyr^f*
389 allele is segregating, attention to the possibility of environmental influences is warranted. 4) *Tyr*
390 has been linked with many ophthalmic traits in mice^{40, 41, 42, 46, 51, 52, 53, 54, 55, 56}, in some instances,
391 a consideration of gene-environment interactions in the mechanism of these various models
392 may be warranted. And finally, 5) our study uncovers a genetic peculiarity. *Cctq1* was originally
393 reported as a single QTL on chromosome 7, detected in an F2 intercross of KS and SJL inbred
394 mice¹⁶. In studies of successive generations of congenic mice, N4F2 mice heterozygous for the
395 *Cctq1* alleles showed the original differential phenotype (over-dominant, *increased* CCT
396 compared to littermate controls)¹⁶, whereas in N10–N15 intercrosses, mice homozygous for the
397 SJL allele showed the differential phenotype (recessive, *decreased* CCT compared to littermate
398 controls). As the sub-congenics were intercrossed and analyzed for CCT, KS.SJL-
399 *Cctq1a^{SJL};Cctq1b^{KS}* mice consistently had thinner corneas than KS.SJL-*Cctq1a^{KS};Cctq1b^{KS}*
400 mice of the same generation, but there were also fluctuations in absolute value related to
401 generation and interval size. The likely explanation for these observations is that there was

402 more than one CCT-modifying gene in the original *Cctq1* interval, which was in fact found to be
403 the case by the resolution of *Cctq1* into *Cctq1a* and *Cctq1b*. This is consistent with the findings
404 of human GWAS, indicating that there are likely hundreds of CCT-influencing genes dispersed
405 throughout the genome, many of which will be physically close to one another. In mice, it is
406 known that as a locus is narrowed using congenics, genes can be segregated away from
407 nearby modifiers and the overall phenotype of the original QTL can be reduced, disappear, or
408 reverse its apparent effect^{57, 58}. The current data seem to exemplify this phenomenon.

409
410 In summary, our phenotype-driven genetic study of CCT identified *Tyr* as a significant regulator
411 of CCT in mice. The molecular findings of this study were unexpected. We propose that the
412 results can be explained by an epiphenomenon whereby a gene:environment interaction; i.e.,
413 *Tyr*-mediated albinism allowing increased exposure of the eye to light has an important
414 influence on corneal development.

415

416 **Materials and Methods**

417

418 **Experimental animals**

419 All animals were treated in accordance with the ARVO Statement for the Use of Animals in
420 Ophthalmic and Vision Research. The majority of mice were housed and bred at the University
421 of Iowa Research Animal Facility with approval for experimental protocols conferred by the
422 Institutional Animal Care and Use Committee of the University of Iowa. Two cohorts of mice, the
423 C57BL/6J (JAX Stock No. 000664) and B6.Cg-*Tyr*^{c-2J}/J (JAX Stock No. 000058) used for in vivo
424 axial length measurements (Figure 7) were purchased from The Jackson Laboratory at 10-
425 weeks-old and subsequently housed at the University of California San Francisco until 12-
426 weeks-old with approval for experimental protocols conferred by the Institutional Animal Care
427 and use Committee at the University of California San Francisco. Mouse strains used in this

428 study include: SJL/J (Stock No. 000686), C57BLKS/J (JAX Stock No. 000662), C57BL/6J (JAX
429 Stock No. 000664), B6.Cg-*Tyr^{c-2J}*/J (JAX Stock No. 000058), B6;129-*Fzd4^{tm1Nat}*/J (JAX Stock
430 No. 012823), B6.Cg-*Tyr^{c-h}*/J (JAX Stock No. 000104; Imported from Dr. Brian Brooks at the
431 NIH), B6.Cg-*Ctsc^{tm1Ley}* (Imported from Dr. Christine Pham at Washington University), KS.Cg-
432 SJL^{*Cctq1*}, B6-*Ctsc^{tm1Mga}*, and B6-*Tyr^{tm4Mga}*. All experiments included male and female mice.

433

434 **Chromosome 7 QTL analysis**

435 The chromosome 7 quantitative trait locus analysis was performed with R/qtl, using the two-
436 dimensional genome-wide scan (scantwo). Significance thresholds were determined empirically
437 by permutation testing, using 1000 permutations. The validity of a multiple QTL model was
438 tested by performing a multiple regression analysis. Phenotypic variance was estimated and the
439 full model was statistically compared to reduced models in which one QTL was dropped.

440

441 **Constructing congenic mice**

442 A ~38.3cM genomic region (*i.e.*, *Cctq1*) spanning from *D7Mit318* (SSLP marker at 42.3 cM) to
443 *rs13479545* (SNP marker at 81.2 cM) was transferred from SJL/J mice (abbreviated throughout
444 as SJL; thick cornea) onto the genetic background of C57BLKS/J mice (abbreviated throughout
445 as KS; thin cornea) by reiterative backcrossing. Mice carrying the SJL alleles within the region
446 (*i.e.*, KS.SJL-*Cctq1^{Het}*) were selected at each generation by using a panel of six markers that
447 were tested and found to be polymorphic between KS and SJL mice. At the N10 generation,
448 mice were intercrossed. At this point, *Cctq1* was treated as a digenic locus, renamed to *Cctq1a*
449 and *Cctq1b* (see Results and Figure 2). *Cctq1a* encompassed the region spanning from
450 *D7Mit318* (42.3 cM) to *D7Mit220* (55.7 cM). *Cctq1b* spanned from *D7Mit105* (70.3 cM) to
451 *rs13479545* (81.2 cM). All genotype combinations of *Cctq1a* and *Cctq1b* (9 possible
452 combinations; *i.e.*, homozygosity for KS alleles, heterozygous, or homozygosity for SJL alleles
453 at each locus) were analyzed for their effect on CCT.

454

455 Sub-congenic mice harboring reduced *Cctq1a* intervals (KS alleles at *Cctq1b*) were also
456 generated. At N12, *Cctq1a* was reduced to a 15.9 cM region spanning from *D7mit347* to
457 *D7mit321*. These N12 sub-congenic mice are referred to throughout as KS.SJL-
458 *Cctq1a*(15.9cM). At N15, *Cctq1a* was reduced to a 9.9 cM region spanning from *rs3672782* to
459 *D7mit321*. These sub-congenic N15 mice are referred to throughout as KS.SJL-*Cctq1a*(9.9cM).
460 Sub-congenic mice were intercrossed, and all genotypes were assessed for the CCT
461 phenotype. The KS.SJL-*Cctq1* line has been sperm cryopreserved.

462

463 **CCT phenotyping**

464 All measurements were recorded from adult mice. Mice were injected with a standard mixture of
465 ketamine/xylazine (intraperitoneal injection of 100 mg ketamine + 10 mg xylazine / kg body
466 weight; Ketaset®, Fort Dodge Animal Health, Fort Dodge, IA; AnaSed®, Lloyd Laboratories,
467 Shenandoah, IA). During induction of anesthesia, mice were provided supplemental indirect
468 warmth by a heating pad. Immediately following anesthesia, eyes were hydrated with balanced
469 salt solution (BSS; Alcon Laboratories, Fort Worth, TX) and corneal images were obtained with
470 a Bioptigen optical coherence tomographer (SD-OCT; Bioptigen, Inc., USA). A 12mm telecentric
471 bore with a reference arm position of 1048 was used to image the anterior segment of each eye.
472 The bore was positioned such that the pupil of the eye was centered in the volume intensity
473 projection. Scan parameters were as follows: radial volume scans 2.0 mm in diameter, 1000 A-
474 scans/B-scan, 100 B-scans/volume, 1 frame/B-scan, and 1 volume. Central corneal thickness
475 (CCT) was measured for each eye using vertical angle-locked B-scan calipers. Mice were
476 included in the analysis if the difference between the right and left eyes was less than 7 μm and
477 if both eyes were free from opacity. The average CCT and standard deviation for each genotype
478 was statistically compared using Student's two-tailed *t*-test for comparison of two cohorts or
479 one-way ANOVA with a Tukey post-test for comparison of three or more cohorts.

480

481 **Recombination mapping**

482 For genetic mapping of the gene underlying *Cctq1a*, additional polymorphic markers were
483 identified and tiled into the region. Intercrosses of N10 mice were continued and mice with
484 informative recombination events were analyzed for the CCT phenotype. Based on the allelic
485 effects of the QTL on the CCT phenotype (see Results), the genomic boundaries of the QTL
486 (and hence, the region of the underlying gene) were deduced by comparing the phenotype of
487 the recombinant mice with the location of the recombination event within the critical interval. The
488 following is a complete list of all the polymorphic markers used for genotyping (listed in order
489 from centromeric to telomeric): *D7Mit318*, *rs13479346*, *rs13479362*, *D7Mit347*, *D7Mit62*,
490 *rs6271685*, *rs108403472*, *Cctq1a-STR5*, *D7Mit31*, *rs3672782*, *rs32438580*, *rs3663323*,
491 *rs13479392*, *rs13479393*, *rs6247100*, *rs13479395*, *D7Mit301*, *D7Mit321*, *D7Mit220*, *D7Mit238*,
492 *D7Mit105*, *rs13479535*, *rs13479536*, and *rs13479545*. Primer sequences are available upon
493 request.

494

495 **Exome sequence analysis**

496 High quality genomic DNA was harvested from KS and SJL spleen tissue using a Qiagen
497 DNeasy Blood and Tissue kit following the manufacturer's instructions; an RNA digestion step
498 was included. DNA samples were sent to BGI Americas for sequencing and passed their quality
499 control standards. Libraries were constructed with an Agilent SureSelect 50Mb Mouse Exome
500 Capture Kit and were sequenced with 50X coverage using an Illumina HiSeq2000. Standard
501 bioinformatics analysis was conducted in which the data was filtered (by removing adaptor
502 contamination and low-quality reads from raw reads), aligned, and SNPs were called and
503 annotated using a reference genome (GRCm38 build).

504

505 **RNASeq analysis**

506 N12F3 KS.SJL-*Cctq1a*(15.9cM)^{KS}, KS.SJL-*Cctq1a*(15.9cM)^{SJL}, and KS inbred mice were
507 euthanized at three weeks of age by cervical dislocation. Immediately upon death, mice were
508 enucleated, and the eyes were placed in RNase free dishes (NEST Biotechnology) containing
509 RNA^{later} RNA stabilization reagent. Corneas from mice were dissected in RNA^{later} and pooled
510 to make one sample (6 corneas per sample); three samples were collected per genotype.
511 Cornea samples were either stored at -80°C in RNA^{later} or processed immediately. Corneas
512 were transferred from RNA^{later} to 0.7 mL of lysis/binding buffer from the *mirVana* miRNA
513 isolation kit (Ambion) and homogenized for 1 minute using a tissue tearer (Biospec Products,
514 Inc.). The homogenate was then passed through a QIAshredder column (Qiagen) and the lysate
515 was collected. For the remainder of the procedure, the samples were processed using the
516 *mirVana* kit for total RNA according to the manufacturer's instructions. The quality and
517 concentration of the RNA was analyzed using a NanoDrop 2000 and the Agilent Model 2100
518 Bioanalyzer. All samples had RNA integrity numbers of 9.5 or greater, indicating high quality
519 RNA with little degradation of the samples. Samples were barcoded and stranded libraries were
520 prepared by the Genomics Division of the Iowa Institute of Human Genetics. The nine libraries
521 were pooled together, split into two equal parts, and run on two lanes of an Illumina HiSeq to
522 obtain 100 base pair, paired-end sequence reads.

523
524 Reads were mapped to the mm10 mouse genome build using Tophat2 (ver 2.0.11; [PMID:
525 23618408]). The '-r' parameter was set to 135, and the '--no-coverage-search' option was used.
526 Transcript abundance was quantified using Cufflinks (ver. 2.1.1; [PMID: PMC3146043]) for
527 RefSeq transcript models from the Illumina iGenomes mm10 package. Ribosomal RNA and
528 mitochondrial gene loci, obtained from UCSC Genome Table Viewer, were masked from the
529 Cufflinks analysis, and the '--max-bundle-frags' parameter was set to 20000000. Differential
530 expression between genotypes was performed using Cuffdiff (ver. 2.1.1; [PMID: 23222703]).
531 Genes identified from each comparison were subsequently filtered for only those with a q-value

532 ≤ 0.001 and a mean FPKM (Fragments Per Kilobase of transcript per Million mapped reads)
533 value ≥ 1 in at least one of the strains. Functional enrichment analysis was performed with
534 WebGestalt [32, 33] with analysis parameters detailed in Supplementary Data 8.

535

536 **Constructing *Ctsc* null mice**

537 B6-*Ctsc*^{KO} mice were generated by the Genome Editing Facility at The University of Iowa on a
538 pure C57BL/6J (JAX Stock No. 000664) background by targeting *Ctsc* Exon 1 with
539 CRISPR/Cas9 using guide sequence: CGTGCGCTCCGACACTCCTGCC. Founders were
540 crossed with C57BL/6J mice and offspring analyzed for germline transmission of *Ctsc*
541 mutations. From four founders, we observed transmission of four separate *Ctsc* mutations, all
542 predicted to be null based on Sanger sequencing results. Three *Ctsc* mutations were
543 propagated in separate intercross mouse lines and were validated as null mutations by Western
544 Blot using an antibody against CTSC (Catalog #AF1034; R&D Systems, Inc.; Minneapolis, MN;
545 Supplementary Data 10). One of these mutations, *Ctsc*^{tm1Mga}, is a 46 bp exon 1 coding
546 sequence deletion that was used for additional downstream analysis.

547

548 **Constructing *Tyr* null mice**

549 To generate mice with *Tyr* null mutations on a pure C57BL/6J (JAX Stock No. 000664)
550 background, the Genome Editing Facility at the University of Iowa targeted *Tyr* Exon 1 with
551 CRISPR/Cas9 using two guide sequences simultaneously: 1) CCATGGATGGGTGATGGGAG
552 and 2) TTCAAAGGGGTGGATGACCG. Founders were crossed with C57BL/6J mice and
553 offspring analyzed by Sanger sequencing for germline transmission of *Tyr* mutations. This
554 experiment generated more alleles than we could reasonably work with (15 unique mutations
555 identified via sequencing; Supplementary Data 12). For each unique mutation, we set up a
556 complementation cross with B6.*Tyr*^{c-2J} and screened progeny coat color for alleles conferring
557 novel function. F1 progeny were screened for 14 alleles; the mice harboring the remaining allele

558 did not produce F1 progeny. All 14 alleles produced a standard albino coat color in trans with
559 the *Tyr^{c-2J}* mutation, indicating failure to complement. Going forward, we chose to complete
560 additional studies for one allele, *Tyr^{Im4Mga}*, which is a 4 bp deletion in the coding sequence of
561 exon 1, causes a frameshift and leads to a premature stop codon predicted to cause RNA-
562 mediated decay (i.e., a presumed null mutation). Accordingly, homozygotes of this strain are
563 albino.

564

565 **L-DOPA supplementation studies**

566 Breeder cages of C57BL/6J, B6.Cg-*Tyr^{c-2J}*/J, and B6.Cg-*Tyr^{c-h}*/J were provided with water
567 bottles containing water only (control) or water with 200mg/L of L-DOPA, with 30mg/L of
568 benserazide to minimize the conversion of L-DOPA to dopamine in the peripheral nervous
569 system. Fresh water bottles were prepared and supplied every Monday, Wednesday, and
570 Friday. Litters were weaned into cages where they continued to receive the same treatment of
571 supplemented water until 13–16 weeks old.

572

573 **Environmental chamber**

574 Breeder cages of C57BL/6J, B6.Cg-*Tyr^{c-2J}*/J, and B6.Cg-*Tyr^{c-h}*/J were housed in rodent
575 environmental control chambers (Powers Scientific) either at 10°C or 32°C and with either a
576 standard light cycle (12 hrs on/12 hrs off) or dark-rearing. Resulting pups were born and group-
577 housed at the altered temperature and light cycle until adulthood, when CCT was analyzed by
578 OCT at 10–15 weeks old.

579

580 **Axial length phenotyping**

581 Envisu R4300 spectral-domain optical coherence tomography (SD-OCT, Leica/Bioptigen Inc.,
582 Research Triangle Park, NC, USA) was employed to measure the ocular axial length in adult

583 (12-week-old) mice⁵⁹. Mice were anesthetized with ketamine/xylazine (100 mg/kg and 5mg/kg,
584 respectively; intraperitoneal) and their eyes dilated before placing the animal in a cylindrical
585 holder. The eye was hydrated with Genteal (Alcon, Fort Worth, TX, USA) and positioned in front
586 of the OCT light source. Correct alignment of the eye was achieved by placing the Purkinje
587 image in the center of the pupil. The images were acquired in rectangular volume and radial
588 volume scans. The axial length was calculated by measuring the distance from the corneal
589 surface to the RPE/choroid interface for both the left and right eyes of a given mouse.
590 Measurements from the left and right eye of each mouse were averaged to give a single
591 measurement per animal. Measurements from all eyes were included in the analysis. To
592 minimize the possible effect of body weight on ocular size, we ensured that body weight of
593 littermates was within a narrow range in each of the comparative groups. The average axial
594 length and standard deviation for each genotype was statistically compared using Student's
595 two-tailed *t*-test.

596

597 **Statistics**

598 A multiple regression analysis, in which each locus and the interaction component were
599 sequentially dropped from the 2-QTL model, was used to analyze the presence of two
600 interacting loci on chromosome 7. Student's two-tailed *t*-test was used to evaluate the difference
601 between two independent genotypes for CCT (*t*-values and degrees of freedom for each
602 comparison are listed in Supplementary Data 5) and axial length (*t*-value = 5.415; degrees of
603 freedom = 38). A one-way ANOVA with a Tukey post-test was used to evaluate the difference
604 between three or more independent genotypes for CCT (*f*-values and degrees of freedom for
605 each comparison are listed in Supplementary Data 5). A one-way ANOVA with Sidak test was
606 used to evaluate four comparisons to determine the effect of two environmental conditions on
607 CCT in B6.cg-*Tyr*^{c-h} and B6.cg-*Tyr*^{c-2J} mice (*f*-value and degrees of freedom are listed in
608 Supplementary Data 5).

609

610 **ACKNOWLEDGEMENTS**

611 The authors would like to thank Karl Broman for analyzing chromosome 7 of our original F2
612 dataset with us. Transgenic mice were generated at the University of Iowa Genome Editing
613 Core Facility directed by William Paradee, PhD and supported in part by grants from the NIH
614 and from the Roy J. and Lucille A. Carver College of Medicine. We wish to thank Norma
615 Sinclair, Patricia Yarolem and Joanne Schwarting for their technical expertise in generating
616 transgenic mice.

617

618 The authors declare no competing interests.

619

620 **AUTHOR CONTRIBUTIONS**

621 K.J.M., D.R.L., and M.G.A. conceived and designed the experiments. K.J.M., D.R.L., C.J.V.,
622 A.H.B., L.M.D., N.P., H.E.M., M.N.A., and M.G.A. performed the experimental work. K.J.M.,
623 D.R.L., and M.G.A. performed experimental data analysis and interpreted the results with
624 contributions from all authors. S.S.W. analyzed the RNA-seq data supervised by T.E.S. W.J.P.
625 constructed the transgenic mice. S.K. performed the axial length experiment supervised by
626 K.S.N. K.W. verified and performed statistical analyses. K.J.M., D.R.L. and M.G.A. wrote the
627 manuscript with input from all authors. M.G.A. supervised the study and provided funding.

628

629

630 **REFERENCES**

631

- 632 1. Pediatric Eye Disease Investigator G, *et al.* Central corneal thickness in children. *Arch*
633 *Ophthalmol* **129**, 1132-1138 (2011).
634
- 635 2. Hashmani N, *et al.* Effect of age, sex, and refractive errors on central corneal thickness
636 measured by Oculus Pentacam((R)). *Clin Ophthalmol* **11**, 1233-1238 (2017).
637
- 638 3. Tayyab A, Masrur A, Afzal F, Iqbal F, Naseem K. Central Corneal Thickness and its
639 Relationship to Intra-Ocular and Epidmiological Determinants. *J Coll Physicians Surg*
640 *Pak* **26**, 494-497 (2016).
641
- 642 4. Brandt JD, Beiser JA, Kass MA, Gordon MO, Ocular Hypertension Treatment Study G.
643 Central Corneal Thickness in the Ocular Hypertension Treatment Study (OHTS).
644 *Ophthalmology* **127**, S72-S81 (2020).
645
- 646 5. La Rosa FA, Gross RL, Orengo-Nania S. Central corneal thickness of Caucasians and
647 African Americans in glaucomatous and nonglaucomatous populations. *Arch Ophthalmol*
648 **119**, 23-27 (2001).
649
- 650 6. Swierkowska J, Gajecka M. Genetic factors influencing the reduction of central corneal
651 thickness in disorders affecting the eye. *Ophthalmic Genet* **38**, 501-510 (2017).
652
- 653 7. Toh T, *et al.* Central corneal thickness is highly heritable: the twin eye studies.
654 *Investigative ophthalmology & visual science* **46**, 3718-3722 (2005).
655
- 656 8. Zheng Y, *et al.* Heritability of central corneal thickness in Chinese: the Guangzhou Twin
657 Eye Study. *Investigative ophthalmology & visual science* **49**, 4303-4307 (2008).
658
- 659 9. Choquet H, *et al.* A multiethnic genome-wide analysis of 44,039 individuals identifies 41
660 new loci associated with central corneal thickness. *Commun Biol* **3**, 301 (2020).
661
- 662 10. Iglesias AI, *et al.* Cross-ancestry genome-wide association analysis of corneal thickness
663 strengthens link between complex and Mendelian eye diseases. *Nat Commun* **9**, 1864
664 (2018).
665
- 666 11. Dhooge T, *et al.* More than meets the eye: Expanding and reviewing the clinical and
667 mutational spectrum of brittle cornea syndrome. *Hum Mutat*, (2021).
668
- 669 12. Lu Y, *et al.* Genome-wide association analyses identify multiple loci associated with
670 central corneal thickness and keratoconus. *Nature genetics* **45**, 155-163 (2013).
671
- 672 13. Lu Y, *et al.* Common genetic variants near the Brittle Cornea Syndrome locus ZNF469
673 influence the blinding disease risk factor central corneal thickness. *PLoS Genet* **6**,
674 e1000947 (2010).

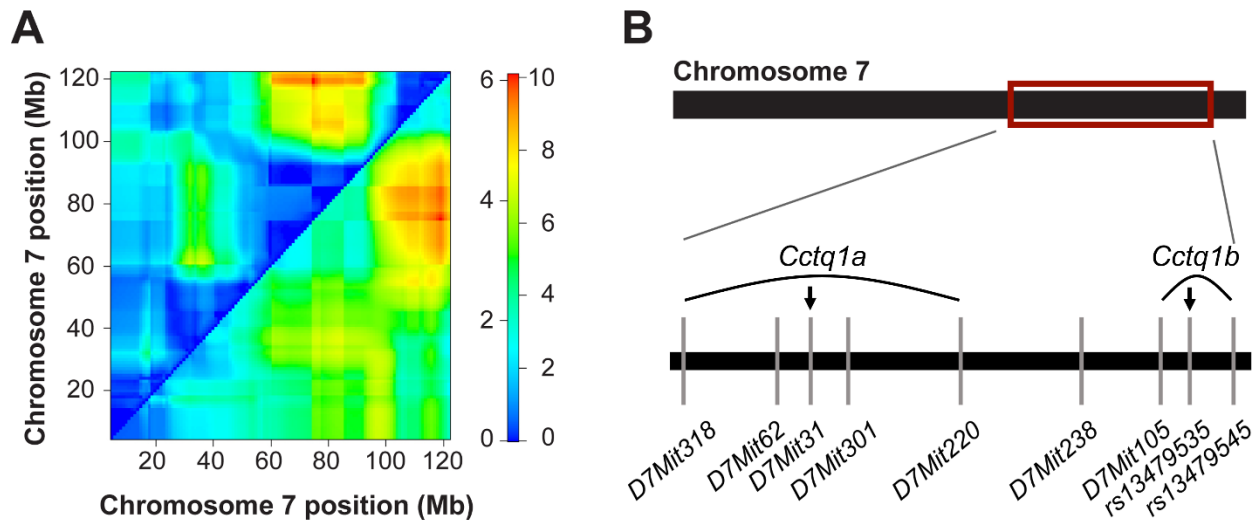
- 675
676 14. Dimasi DP, *et al.* Novel quantitative trait loci for central corneal thickness identified by
677 candidate gene analysis of osteogenesis imperfecta genes. *Hum Genet* **127**, 33-44 (2010).
678
679 15. Zhang J, Wu D, Dai Y, Xu J. Functional relevance for central cornea thickness-associated
680 genetic variants by using integrative analyses. *BioData Min* **11**, 19 (2018).
681
682 16. Lively GD, Koehn D, Hedberg-Buenz A, Wang K, Anderson MG. Quantitative trait loci
683 associated with murine central corneal thickness. *Physiological genomics* **42**, 281-286
684 (2010).
685
686 17. Lively GD, *et al.* Genetic Dependence of Central Corneal Thickness among Inbred
687 Strains of Mice. *Investigative ophthalmology & visual science* **51**, 160-171 (2010).
688
689 18. Broman KW, Sen S. *A Guide to QTL Mapping with R/qlt*. Springer Science+Business
690 Media (2009).
691
692 19. Broman KW, Wu H, Sen S, Churchill GA. R/qlt: QTL mapping in experimental crosses.
693 *Bioinformatics* **19**, 889-890 (2003).
694
695 20. Wynn EH, Sanchez-Andrade G, Carss KJ, Logan DW. Genomic variation in the
696 vomeronasal receptor gene repertoires of inbred mice. *BMC Genomics* **13**, 415 (2012).
697
698 21. Liao Y, Wang J, Jaehnig EJ, Shi Z, Zhang B. WebGestalt 2019: gene set analysis toolkit
699 with revamped UIs and APIs. *Nucleic acids research* **47**, W199-W205 (2019).
700
701 22. Wang Y, Huso D, Cahill H, Ryugo D, Nathans J. Progressive cerebellar, auditory, and
702 esophageal dysfunction caused by targeted disruption of the frizzled-4 gene. *J Neurosci*
703 **21**, 4761-4771 (2001).
704
705 23. Pham CT, Ley TJ. Dipeptidyl peptidase I is required for the processing and activation of
706 granzymes A and B in vivo. *Proc Natl Acad Sci U S A* **96**, 8627-8632 (1999).
707
708 24. Le Fur N, Kelsall SR, Mintz B. Base substitution at different alternative splice donor sites
709 of the tyrosinase gene in murine albinism. *Genomics* **37**, 245-248 (1996).
710
711 25. Green EL. Albino-2J (c<2J>). *Mouse News Lett* **49**, (1973).
712
713 26. Beermann F, Orlow SJ, Lamoreux ML. The Tyr (albino) locus of the laboratory mouse.
714 *Mamm Genome* **15**, 749-758 (2004).
715
716 27. Zhou X, Pardue MT, Iuvone PM, Qu J. Dopamine signaling and myopia development:
717 What are the key challenges. *Prog Retin Eye Res* **61**, 60-71 (2017).
718
719 28. Feldkaemper M, Schaeffel F. An updated view on the role of dopamine in myopia. *Exp*
720 *Eye Res* **114**, 106-119 (2013).

- 721
722 29. Bergen MA, *et al.* Altered Refractive Development in Mice With Reduced Levels of
723 Retinal Dopamine. *Investigative ophthalmology & visual science* **57**, 4412-4419 (2016).
724
725 30. Kidson S, Fabian B. Pigment synthesis in the Himalayan mouse. *J Exp Zool* **210**, 145-152
726 (1979).
727
728 31. Kwon BS, Halaban R, Chintamaneni C. Molecular basis of mouse Himalayan mutation.
729 *Biochem Biophys Res Commun* **161**, 252-260 (1989).
730
731 32. Tkatchenko TV, *et al.* Photopic visual input is necessary for emmetropization in mice.
732 *Exp Eye Res* **115**, 87-95 (2013).
733
734 33. Allen GM. The heredity of coat color in mice. *Proceedings of the American Academy of*
735 *Arts and Sciences* **40**, 61-163 (1904).
736
737 34. Castle WE, Allen GM. The heredity of albinism. *Proceedings of the American Academy*
738 *of Arts and Sciences* **38**, 603-622 (1903).
739
740 35. Seruggia D, Josa S, Fernandez A, Montoliu L. The structure and function of the mouse
741 tyrosinase locus. *Pigment Cell Melanoma Res*, (2020).
742
743 36. Hanlon SD, Patel NB, Burns AR. Assessment of postnatal corneal development in the
744 C57BL/6 mouse using spectral domain optical coherence tomography and microwave-
745 assisted histology. *Exp Eye Res* **93**, 363-370 (2011).
746
747 37. Chakraborty R, Ostrin LA, Benavente-Perez A, Verkicharla PK. Optical mechanisms
748 regulating emmetropisation and refractive errors: evidence from animal models. *Clin Exp*
749 *Optom* **103**, 55-67 (2020).
750
751 38. Mohawk JA, Green CB, Takahashi JS. Central and peripheral circadian clocks in
752 mammals. *Annu Rev Neurosci* **35**, 445-462 (2012).
753
754 39. Peirson SN, Brown LA, Potheary CA, Benson LA, Fisk AS. Light and the laboratory
755 mouse. *J Neurosci Methods* **300**, 26-36 (2018).
756
757 40. Steininger TL, Rye DB, Gilliland MA, Wainer BH, Benca RM. Differences in the
758 retinohypothalamic tract in albino Lewis versus brown Norway rat strains. *Neuroscience*
759 **54**, 11-14 (1993).
760
761 41. Miller AM, Chappell R, Obermeyer WH, Benca RM. Analysis of the retinohypothalamic
762 tract in congenic albino and pigmented rats. *Brain Res* **741**, 348-351 (1996).
763
764 42. Fleming MD, Benca RM, Behan M. Retinal projections to the subcortical visual system
765 in congenic albino and pigmented rats. *Neuroscience* **143**, 895-904 (2006).
766

- 767 43. Chakraborty R, Ostrin LA, Nickla DL, Iuvone PM, Pardue MT, Stone RA. Circadian
768 rhythms, refractive development, and myopia. *Ophthalmic Physiol Opt* **38**, 217-245
769 (2018).
770
- 771 44. Lopez VM, Decatur CL, Stamer WD, Lynch RM, McKay BS. L-DOPA is an endogenous
772 ligand for OA1. *PLoS Biol* **6**, e236 (2008).
773
- 774 45. Korshunov KS, Blakemore LJ, Trombley PQ. Dopamine: A Modulator of Circadian
775 Rhythms in the Central Nervous System. *Front Cell Neurosci* **11**, 91 (2017).
776
- 777 46. Libby RT, *et al.* Modification of ocular defects in mouse developmental glaucoma
778 models by tyrosinase. *Science* **299**, 1578-1581 (2003).
779
- 780 47. Lee H, Scott J, Griffiths H, Self JE, Lotery A. Oral levodopa rescues retinal morphology
781 and visual function in a murine model of human albinism. *Pigment Cell Melanoma Res*
782 **32**, 657-671 (2019).
783
- 784 48. Kirkwood BJ. Albinism and its implications with vision. *Insight* **34**, 13-16 (2009).
785
- 786 49. Rao VA, Swathi P, Chaitra, Thappa DM. Bilateral keratoconus with oculocutaneous
787 albinism. *Indian J Dermatol Venereol Leprol* **74**, 407-409 (2008).
788
- 789 50. Dimasi DP, *et al.* Ethnic and mouse strain differences in central corneal thickness and
790 association with pigmentation phenotype. *PLoS One* **6**, e22103 (2011).
791
- 792 51. Buttner C, *et al.* Tyrosinase Is a Novel Endogenous Regulator of Developmental and
793 Inflammatory Lymphangiogenesis. *Am J Pathol* **189**, 440-448 (2019).
794
- 795 52. Mason C, Slavi N. Retinal Ganglion Cell Axon Wiring Establishing the Binocular
796 Circuit. *Annu Rev Vis Sci* **6**, 215-236 (2020).
797
- 798 53. Savinova OV, *et al.* Intraocular pressure in genetically distinct mice: an update and strain
799 survey. *BMC Genet* **2**, 12 (2001).
800
- 801 54. Johnson BA, Cole BS, Geisert EE, Ikeda S, Ikeda A. Tyrosinase is the modifier of
802 retinoschisis in mice. *Genetics* **186**, 1337-1344 (2010).
803
- 804 55. Anderson MG, *et al.* Genetic context determines susceptibility to intraocular pressure
805 elevation in a mouse pigmentary glaucoma. *BMC Biol* **4**, 20 (2006).
806
- 807 56. Oh J, *et al.* Genetic background-dependent role of Egr1 for eyelid development. *Proc*
808 *Natl Acad Sci U S A* **114**, E7131-E7139 (2017).
809
- 810 57. Mott R, Flint J. Dissecting quantitative traits in mice. *Annual review of genomics and*
811 *human genetics* **14**, 421-439 (2013).
812

- 813 58. Solberg Woods LC. QTL mapping in outbred populations: successes and challenges.
814 *Physiological genomics* **46**, 81-90 (2014).
815
- 816 59. Paylakhi S, *et al.* Muller glia-derived PRSS56 is required to sustain ocular axial growth
817 and prevent refractive error. *PLoS Genet* **14**, e1007244 (2018).
818
819
- 820

821 **Figure 1. *Cctq1* contains two adjacent interacting QTL, *Cctq1a* and *Cctq1b*.** A) The
822 chromosome 7 pairwise scan identified a potential interaction between *D7Mit31* and
823 *rs13479535* (full LOD score = 10.33, interactive LOD score = 5.05). The *upper left triangle*
824 displays the interactive LOD score (LOD_{i_i} ; left side of the heat map scale) and the *lower right*
825 *triangle* displays the full LOD score (LOD_{i_i} ; right side of the heat map scale). Chromosome 7
826 positions (Mb) are based on NCBI Build 33. B) Genetic map of chromosome 7 showing the
827 *Cctq1a* and *Cctq1b* loci. The area boxed in red is the original *Cctq1* interval blown up to show
828 the intervals of *Cctq1a* and *Cctq1b*, and a subset of the polymorphic markers used for
829 genotyping. The arrows indicate the peaks of the two QTL.
830



831

832 **Table 1. CCT phenotype results of adult N10F2 mice.**

833

<i>Cctq1a</i> ^a	<i>Cctq1b</i> ^a	Avg. CCT ± StDev. ^b	# Mice
KS	KS	94.8 ± 2.4	13
KS	Het	93.3 ± 2.5	13
KS	SJL	90.8 ± 2.6	13
Het	KS	95.5 ± 2.9	13
Het	Het	96.2 ± 3.4	13
Het	SJL	97.0 ± 2.3	13
SJL	KS	88.1 ± 3.7*	13
SJL	Het	86.8 ± 4.2*	13
SJL	SJL	88.8 ± 3.6*	13

834

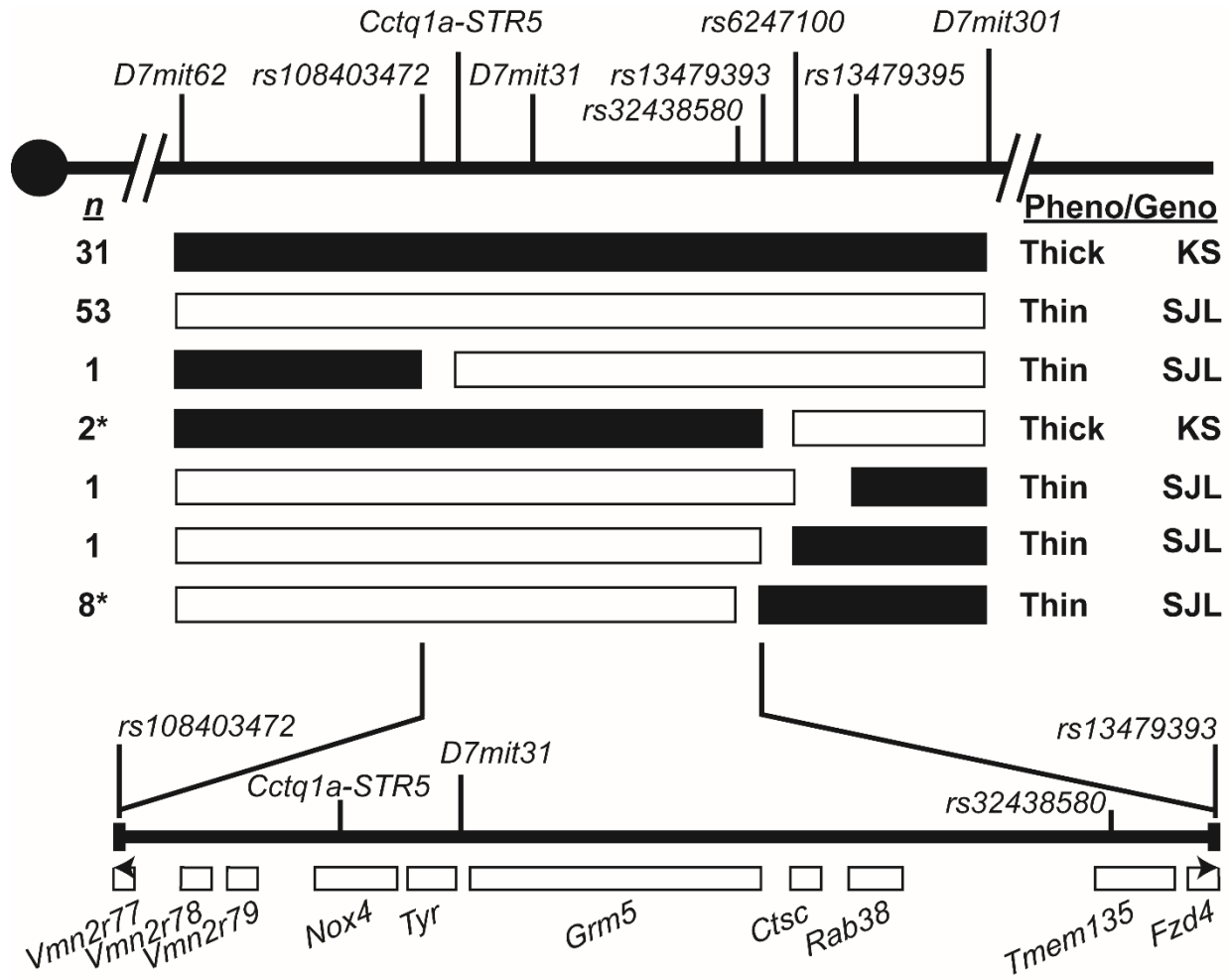
835 ^a KS, homozygous for KS alleles across the indicated QTL; Het, heterozygous for alleles across

836 the indicated QTL; SJL, homozygous for SJL alleles across the indicated QTL

837 ^b Asterisk (*), significantly different ($p < 0.01$) than inbred KS mice by one-way ANOVA with

838 Tukey post-test

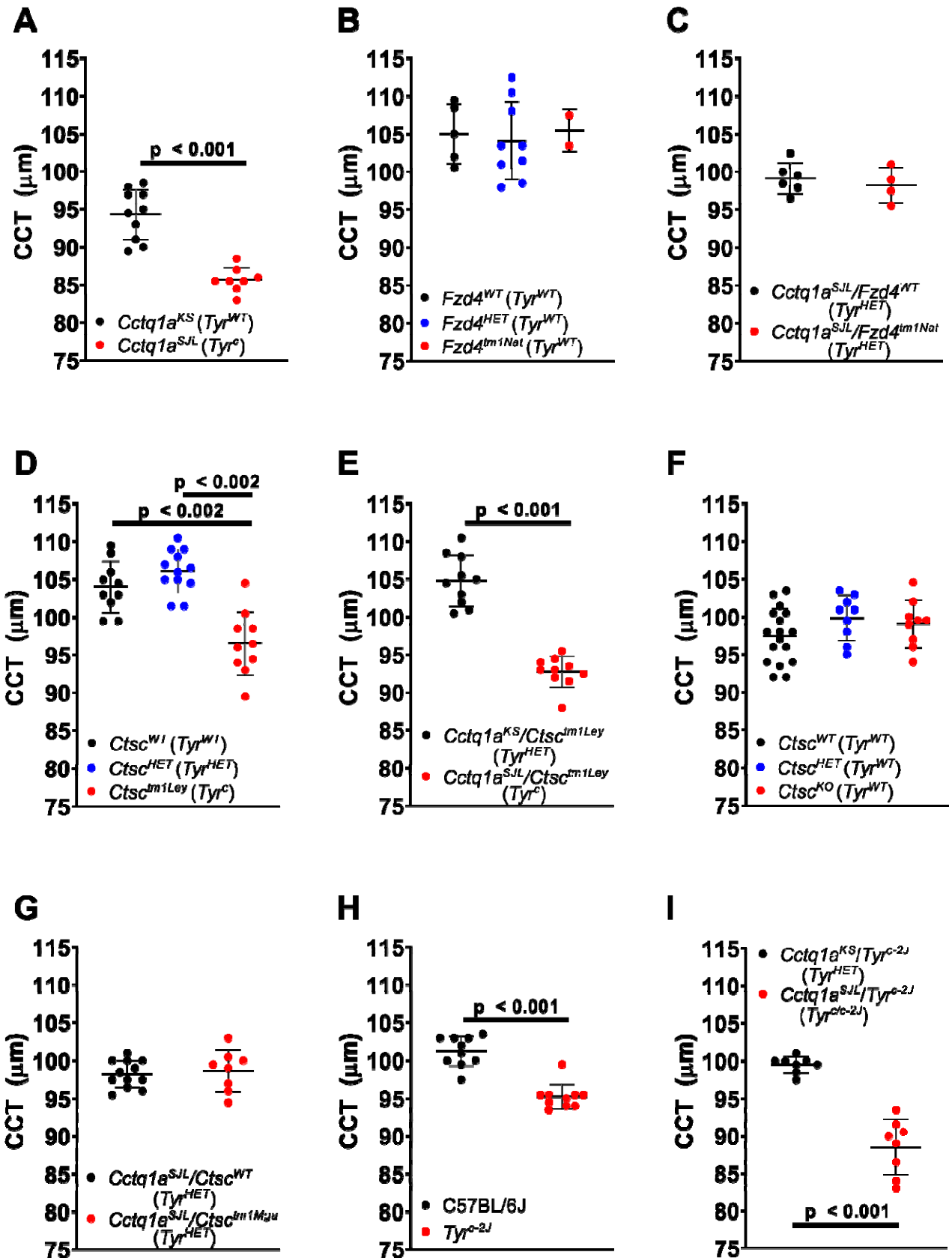
839 **Figure 2. Genetic mapping of *Cctq1a* on mouse chromosome 7 using intercrosses of**
840 **KS.SJL-*Cctq1a* congenic and sub-congenic mice.** *Black boxes* represent the KS or HET
841 genotype associated with a thick cornea and *white boxes* represent the SJL genotype
842 associated with a thin cornea. The number of mice (*n*) with each haplotype is listed to the left of
843 each row, with progeny-tested mice denoted with an asterisk (*). The adult CCT phenotype
844 (*pheno*; measured by optical coherence tomography) relative to littermate controls and the
845 deduced genotype (*geno*) for each haplotype is listed to the right of each row as “Thick KS” or
846 “Thin SJL”. The *vertical lines* across the chromosome represent markers that are polymorphic
847 between KS and SJL mice. Using mice with informative recombinations, the gene underlying
848 *Cctq1a* was narrowed to the region between *rs108403472* and *rs13479393*, which contains
849 seven full genes, *Vmn2r78*, *Vmn2r79*, *Nox4*, *Tyr*, *Grm5*, *Ctsc*, *Rab38*, and *Tmem135*, as well as
850 the 3' portion of *Vmn2r77* and the 5' portion of *Fzd4* (*black arrowheads* indicate partial genes).
851



852

853 **Figure 3. Testing the influence of *Cctq1a* lead positional candidate genes on central**
854 **corneal thickness (CCT).** Each point on the graph represents the average CCT measured by
855 optical coherence tomography from one adult mouse with age-matching across genotypes and
856 *error bars* = mean \pm standard deviation. A) Homozygosity of *Cctq1a*^{SJL} (*red points*) in KS.SJL-
857 *Cctq1a* N15F7 sub-congenic mice results in a significantly decreased CCT compared to
858 littermate controls having *Cctq1a*^{KS} (*black points*) genotypes ($p < 0.001$; Student's two-tailed *t*-
859 test; 12–13 weeks old). B) The *Fzd4*^{tm1Nat} allele has no effect on CCT, in neither the
860 heterozygous (HET; *blue points*) nor homozygous state (*red points*), compared to *Fzd4* wild-
861 type (WT; *black points*) littermate controls (12–13 weeks old). C) The *Fzd4*^{tm1Nat} allele in trans
862 with a *Cctq1a*^{SJL} allele (*red points*) has no effect on (complements) CCT compared to littermate
863 controls having a *Fzd4*^{WT} allele in trans with a *Cctq1a*^{SJL} allele (*black points*; 17–33 weeks old).
864 D) Homozygosity of the *Ctsc*^{tm1Ley} allele (*red points*) results in a significantly decreased CCT
865 compared to littermate controls (HET = *blue points*; WT = *black points*; $p < 0.002$ for each
866 comparison to homozygotes; one-way ANOVA with Tukey post-test; 11 weeks old). E) The
867 *Ctsc*^{tm1Ley} allele in trans with a *Cctq1a*^{SJL} allele (*red points*) results in a significantly decreased
868 (fails to complement) CCT compared to littermate controls having a *Ctsc*^{tm1Ley} allele in trans with
869 a *Cctq1a*^{KS} allele (*black points*; $p < 0.001$ Student's two-tailed *t*-test; 15–18 weeks old). F)
870 *Ctsc*^{KO} mice on a pure B6 background, harboring one of four *tmMga* alleles (*red points*)
871 predicted to result in a null protein, have an unchanged CCT compared to *Ctsc*^{WT} (*black points*)
872 or *Ctsc*^{HET} (*blue points*) littermate controls (10–12 weeks old). G) The *Ctsc*^{tm1Mga} allele, made on
873 a pure B6 background, in trans with a *Cctq1a*^{SJL} allele (*red points*) has no effect on
874 (complements) CCT compared to littermate controls having a *Ctsc*^{WT} allele in trans with a
875 *Cctq1a*^{SJL} allele (*black points*; 10–11 weeks old). H) Homozygosity of the *Tyr*^{c-2J} allele (*red*
876 *points*) results in a significantly decreased CCT compared to C57BL/6J mice (*black points*; $p <$
877 0.001 ; Student's two-tailed *t*-test; 11–13 weeks old). I) The *Tyr*^{c-2J} allele in trans with a *Cctq1a*^{SJL}
878 allele (*red points*) results in a significantly decreased (fails to complement) CCT compared to

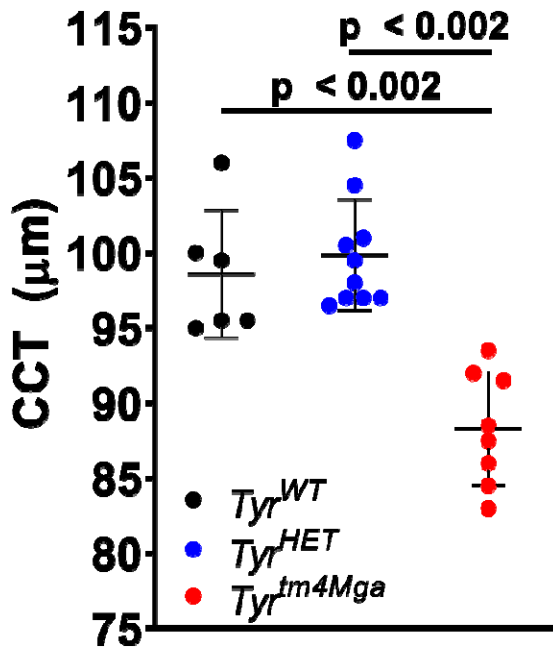
- 879 littermate controls having a Tyr^{p-2J} allele in trans with a $Cctq1a^{KS}$ allele (*black points*; $p < 0.001$;
- 880 Student's two-tailed t -test; 10–12 weeks old).



883 **Figure 4. A null mutation in *Tyr* results in decreased central corneal thickness (CCT).**

884 Each point on the graph represents the average CCT measured by optical coherence
885 tomography from one adult mouse, 13–17 weeks old, with age-matching across genotypes and
886 error bars = mean \pm standard deviation. Homozygosity of the *Tyr*^{tm4Mga} allele (red points) on a
887 pure C57BL/6J background results in a significantly decreased CCT compared to littermate
888 controls with heterozygous (HET; blue points) or wild-type (WT; black points) alleles ($p < 0.002$
889 for each comparison to homozygotes; one-way ANOVA with Tukey post-test).

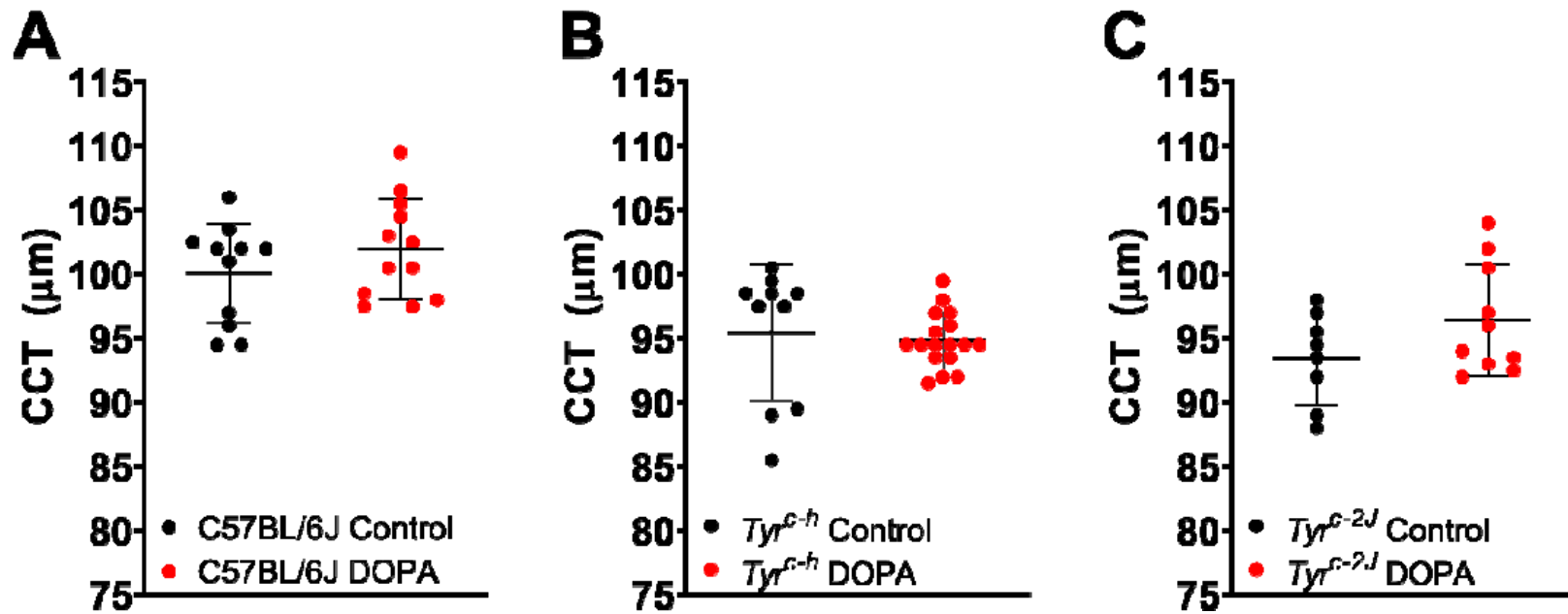
890



891
892

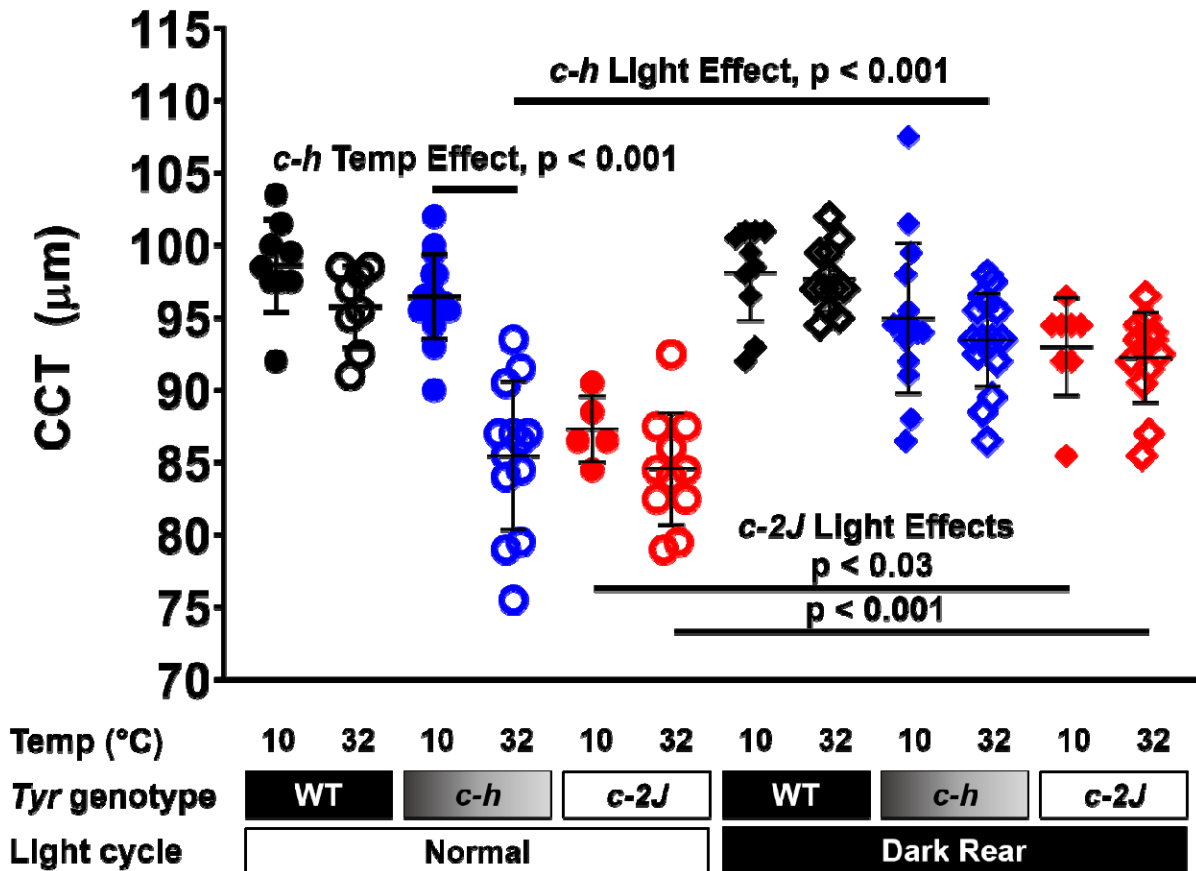
1 **Figure 5. Testing the influence of DOPA on central corneal thickness (CCT).** Each point on the graph represents the average
2 CCT measured by optical coherence tomography from one adult mouse, 13–16 weeks old, with age-matching across genotypes and
3 *error bars* = mean \pm standard deviation. Supplemental DOPA supplied in the drinking water from conception through 10-weeks-old
4 has no significant effect on CCT compared to controls in A) C57BL/6J mice, B) *Tyr^{C-h}* mice, or C) *Tyr^{C-2J}* mice.

5



6

1 **Figure 6. The thin central corneal thickness (CCT) of *c-h* mice raised at increased**
 2 **temperature is rescued by raising *c-h* mice at decreased temperature or by dark-rearing.**
 3 Each point on the graph represents the average CCT measured by optical coherence
 4 tomography from one adult mouse, 10–15 weeks old, with age-matching across genotypes and
 5 *error bars* = mean \pm standard deviation. Cohorts were subjected to standard lighting (*circles*) or
 6 dark-rearing (*diamonds*). Each grouping of *Tyr* genotypes (*black* = WT B6; *blue* = *c-h*
 7 temperature sensitive himalayan; *red* = *c-2J* albino) has mice raised at 10°C (*closed points*) or
 8 32°C (*open points*). Note that cold-rearing or dark-rearing *c-h* mice have similar effects that are
 9 each statistically significant and that dark-rearing *c-2J* mice significantly changes CCT (one-way
 10 ANOVA with Sidak test).



11

1 **Figure 7. *Tyr* influences ocular axial length.** Each point on the graph represents the average
2 axial length measured by optical coherence tomography from one 12-week-old adult mouse and
3 error bars = mean \pm standard deviation. Axial length differences between C57BL/6J (black
4 points) and *Tyr*^{c-2J} (red points) mice, measured from the outer surface of the cornea to the
5 retinal pigment epithelium/choroid interface, are statistically significant ($p < 0.001$; Student's
6 two-tailed *t*-test).

7

